Structure and Redox Properties of $Ce_xTi_{1-x}O_2$ Solid Solution

Mengfei Luo,[†] Jun Chen,[†] Linshen Chen,[‡] Jiqing Lu,[†] Zhaochi Feng,[†] and Can Li*,[†]

State Key Laboratory of Catalysis, Dalian Institute of Chemical Physics, Chinese Academy of Sciences, Dalian 116023, China, and Central Laboratory, Zhejiang University, Hangzhou 310028, China

A series of $Ce_xTi_{1-x}O_2$ mixed oxide materials was synthesized by a sol−gel method with *x* varying from 0.1 to 0.9 and characterized by XRD, Raman, and TPR techniques. The structure of the mixed oxides changes with the Ce/Ti ratio. When the *x* value is decreased from 1.0 to 0.6 for $Ce_xTi_{1-x}O_2$, only a cubic phase is detected, and the lattice parameter of the cubic phase decreases because of the formation of a solid solution by substituting Ti atoms into a CeO_2 lattice. When $x = 0.3$, a new phase is observed. The structure of this new phase was characterized by Rietveld refinement of X-ray diffraction data. This mixed oxide adopts the monoclinic symmetry with the space group $C2/m$ and $a = 0.9811(8)$ nm, $b = 0.3726(3)$ nm, $c = 0.6831(6)$ nm, and $\beta = 118.84°$. When $x = 0.4$ and 0.5, a mixed phase region is detected. The addition of Ti atoms into CeO_2 significantly improves the storage capacity of mobile oxygen of CeO_2 by increasing the reduction extent of the mixed oxides. When $x = 0.3−0.6$, the valence value of Ce after a TPR run is estimated to be close to +3, which obviously is smaller than that for reduced CeO_2 alone. The $Ce_{0.5}Ti_{0.5}O_2$ sample shows the highest capacity of storage oxygen among $Ce_xTi_{1-x}O_2$ mixed oxides. The capacity for reoxidation of the reduced CeO_2-rich solid solution is higher than that of CeO_2-lean mixed oxides. $Ce_xTi_{1-x}O_2$ mixed oxides are promising materials for oxygen storage as well as catalysts for many reactions involving oxygen, such as the catalysts for a three-way reaction to reduce the pollutant emissions or combustion of volatile organic compounds.

1. Introduction

Ceria (CeO_2) has been extensively studied in recent years because of its wide applications in many areas of chemistry. In catalysis, for example, CeO_2 has been used as an important component of automotive three-way catalysts (TWCs) for reducing the exhaust pollutants. The main roles of ceria in three-way catalysis are to promote the noble metal dispersion,[1] increase the thermal stability of the Al_2O_3 support,[2,3] promote CO oxidation and water−gas shift reaction,[4−6] and store/release oxygen as an oxygen reservoir.[7−10] Among these functions, the most important property of CeO_2 is as an oxygen reservoir, which stores and releases oxygen via the redox shift between Ce^{4+} and Ce^{3+} under oxidizing and reducing conditions, respectively. However, a major drawback of CeO_2 is the loss of oxygen storage capability (OSC) due to its sintering at higher temperatures, which leads to the deactivation of the catalyst.[11] Therefore, a great number of CeO_2-based mixed oxide systems (e.g., CeO_2−Al_2O_3,[12] CeO_2−SiO_2,[13] CeO_2−La_2O_3,[12] CeO_2−HfO_2,[14] and CeO_2−ZrO_2[15]) have been investigated with the aim to increase the thermal stability and the OSC of CeO_2. Many studies have shown that the redox properties can be considerably enhanced if additional elements are introduced into the CeO_2 lattice and solid solutions are formed.[15]

Among the CeO_2-containing solid solutions, special attention has been focused on the CeO_2−ZrO_2 solid

* To whom correspondence should be addressed. Tel.: 86-411-4671991, ext. 728, 726. Fax: 86-411-4694447 or 4691570. E-mail: canli@ms.dicp.ac.cn.
† Chinese Academy of Sciences.
‡ Zhejiang University.
(1) Normand, F. L.; Hilaire, K.; Kili, K.; Maire, G. *J. Phys. Chem.* **1988**, *92*, 2561.
(2) Harrison, B.; Diwell, A. F.; Hallett, C. *Plat. Met. Rev.* **1988**, *32*, 73.
(3) Ozawa, M.; Kimura, M. *J. Mater. Sci. Lett.* **1990**, *9*, 291.
(4) Numan, J. G.; Robota, H. J.; Cohn, M. J.; Bradley, S. A. *J. Catal.* **1992**, *133*, 309.
(5) Serre, C.; Garin, F.; Belot, G.; Maire, G. *J. Catal.* **1993**, *141*, 1.
(6) Luo, M.-F.; Hou, Z.-Y.; Yuan, X.-X.; Zheng, X.-M. *Catal. Lett.* **1998**, *50*, 205.
(7) Imamura, S.; Shono, M.; Okamoto, N.; Hamada, A.; Ishida, S. *Appl. Catal. A* **1996**, *142*, 279.
(8) Kacimi, S.; Barbier, J., Jr.; Taha, R.; Duprez, D. *Catal. Lett.* **1993**, *22*, 343.
(9) Zafiris, G. S.; Gorte, R. J. *J. Catal.* **1993**, *143*, 86.
(10) Padeste, C.; Cant, N. W.; Trimm, D. L. *Catal. Lett.* **1993**, *18*, 305.
(11) Schming, S. J.; Belton, D. N. *Appl. Catal. B* **1995**, *6*, 127.
(12) Usmen, R. K.; Graham, G. W.; Watkins, W. L. H.; McCabe, R. W. *Catal. Lett.* **1995**, *30*, 53.
(13) Bensalem, A.; Bozon Verduraz, F.; Delamar, M.; Bugli, G. *Appl. Catal. A* **1995**, *121*, 81.
(14) Zamar, F.; Trovarelli, A.; de Leitenburg, C.; Dolcetti, G. *J. Chem. Soc., Chem. Commun.* **1995**, 965.
(15) Kaspar, J.; Fornasiero, P.; Graziani, M. *Catal. Today* **1999**, *50*, 285.

solution because this material has been found to be very important to the three-way catalyst for eliminating the exhaust gases. From the reported results, the CeO_2–ZrO_2 solid solution shows enhanced thermal stability,[16] redox,[17–19] and catalytic properties[14,20] compared to single ceria. The CeO_2–ZrO_2 mixed oxides have been shown to have high structural stability and oxygen storage capability over a wide range of ceria content. However, few studies were reported on other CeO_2-containing materials.

The aim of this work is to synthesize new CeO_2-containing materials and to investigate their structure and catalytic properties. In this article, we present one of the examples of our trial, $Ce_xTi_{1-x}O_2$ mixed oxides, which shows a very high capability for oxygen storage and is a promising new material for three-way catalysis or other forms of catalysis for oxidation reactions.

2. Experimental Section

2.1. Preparation of $Ce_xTi_{1-x}O_2$ Mixed Oxides. $Ce_xTi_{1-x}O_2$ ($x = 0$–1.0 with an interval of 0.1) mixed oxide samples were prepared by the sol–gel method. A solution of $Ti[O(CH_2)_3CH_3]_4$ and ethanol was added to another solution of $Ce(NO_3)_3 \cdot 6H_2O$ and ethanol under stirring. The solution was slowly gelled after finishing the reaction between $Ti[O(CH_2)_3CH_3]_4$ and H_2O. The gel was dried at 100 °C under stirring and then calcined at 650 °C for 4 h.

2.2. X-ray Powder Diffraction (XRD). XRD patterns were collected on a Rigaku Rotaflex (RU-200B) powder diffractometer equipped with a Cu target and a Ni grating monochromatic system. The working voltage of the instrument was 40 kV and the current was 50 mA. The mean crystallite size of the cubic phase was calculated from the Scherrer equation, where the Scherrer constant (particle shape factor) was taken as 0.89. The lattice parameters were calculated by the least-squares method according to the Cohen procedure.[21] For the $Ce_{0.3}Ti_{0.7}O_2$ sample, the XRD pattern was analyzed by the Rietvald method.[22]

2.3. Laser Raman Spectra. Visible laser Raman spectra were recorded on a Jobin Yvon double monochromator (U-1000) coupled to a photomutiplier tube (PMT) detector and the laser line at 532 nm was used as the excitation source.

2.4. Temperature-Programmed Reduction (TPR). TPR of the mixed oxides was carried out using 10% H_2 in an Ar flow as the reducing agent. The amount of consumed H_2 during the reduction was estimated on the basis of the analysis with a thermal conductivity detector. The gas flow rate was 30 mL/min. The weight of the sample was 25 mg, and the heating rate of TPR was 20 °C/min. Water produced during TPR was trapped in a molecular sieve (5 Å). The extent of reduction was quantitatively calculated according to the TPR peak areas and the result was calibrated on the basis of the hydrogen consumption from the reduction of CuO to Cu.[19]

The sample after a TPR run was reoxidized and then a second TPR run was performed with the purpose of revealing the redox properties of the sample. The first TPR run was carried out up to 950 °C, and subsequently, the sample was cooled to a desired temperature (100, 300, or 500 °C) in the
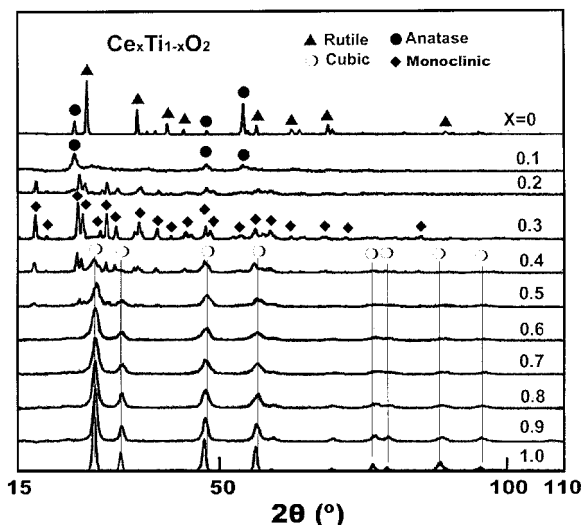
(16) Pijolat, M.; Prin, M.; Soustelle, M.; Touret, O.; Nortier, P. *J. Chem. Soc., Faraday Trans.* **1995**, *91*, 3941.

(17) Fornasiero, P.; Balducci, G.; Di Monte, R.; Kaspar, J.; Sergo, V.; Gubitosa, G.; Ferrero, A.; Graziani, M. *J. Catal.* **1996**, *164*, 173.

(18) Luo, M.-F.; Zheng, X.-M. *Appl. Catal. A* **1999**, *189*, 15.

(19) Trovarelli, A.; Zamar, F.; Llorca, J.; de Leitenburg, C.; Dolcetti, G.; Kiss, J. T. *J. Catal.* **1997**, *169*, 490.

(20) Luo, M.-F.; Zhong, Y.-J.; Wu, T.-H.; Zheng, X.-M. *J. Mater. Sci. Lett.* **1998**, *17*, 1153.

(21) Klug, H. P.; Alexander, L. E. *X-ray Diffraction Procedures*; John Wiley: New York, 1954.

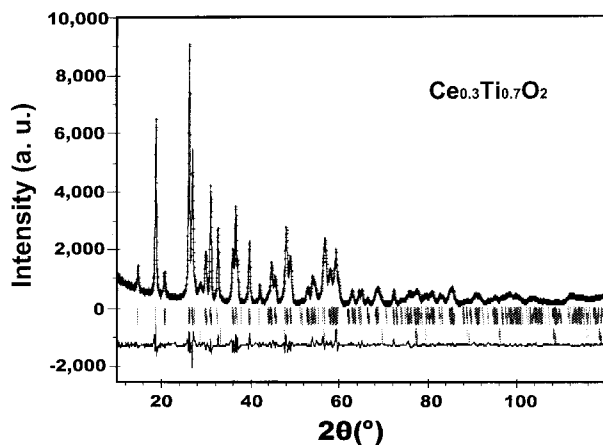(22) Young, R. A. *The Rietveld Method*; Oxford Science Publication: Oxford, 1993; p 22.

Figure 1. XRD patterns of $Ce_xTi_{1-x}O_2$ samples.

H_2 atmosphere. Then, the reduced sample was exposed to air at 100, 300, or 500 °C for 0.5 h. Finally, the sample was cooled to 50 °C in air for the second TPR experiment.

3. Results and Discussion

3.1. Structural Characterization of $Ce_xTi_{1-x}O_2$ Samples. Figure 1 shows the XRD patterns of $Ce_xTi_{1-x}O_2$ mixed oxides calcined at 650 °C. Crystalline phases were identified by comparing with ICDD files (anatase TiO_2, 21-1272; rutile TiO_2. 21-1276; CeO_2, 34-394). From Figure 1, mixed phases, rutile and anatase, are observed for TiO_2, while only the anatase phase is observed for $Ce_{0.1}Ti_{0.9}O_2$. This result means that the addition of a small amount of CeO_2 into TiO_2 inhibits the phase transition from anatase to rutile. This is a very interesting finding that the anatase phase can be stabilized in the presence of a small amount of CeO_2 because rutile is known to be the most stable crystalline phase of TiO_2. For the $Ce_{0.3}Ti_{0.7}O_2$ sample, the diffraction peaks cannot be attributed to any known Ti-containing or Ce-contained mixed oxides according to the current available ICDD files. Therefore, the structure and lattice parameters for the $Ce_{0.3}Ti_{0.7}O_2$ sample were determined by the Retiveld method. The agreement between the experimental and calculated powder X-ray diffraction pattern in the final refinement is shown in Figure 2. Good agreement is found between the experimental and calculated powder X-ray diffraction patterns. $Ce_{0.3}Ti_{0.7}O_2$ exists mainly in a monoclinic phase belonging to the space group $C2/m$ with the lattice parameters $a = 0.9811(8)$ nm, $b = 0.3726(3)$ nm, $c = 0.6831(6)$ nm, and $\beta = 118.84°$. For the $Ce_{0.2}Ti_{0.8}O_2$ sample, the weak diffraction peaks of the anatase phase are observed, except for the diffraction peaks of $Ce_{0.3}Ti_{0.7}O_2$. For $Ce_{0.4}Ti_{0.6}O_2$ and $Ce_{0.5}Ti_{0.5}O_2$ samples, both cubic and monoclinic phases are also observed. It is clear that the addition of CeO_2 into TiO_2 leads to the formation of a monoclinic phase. According to the above results, $Ce_xTi_{1-x}O_2$ samples in the region $0.2 \leq x \leq 0.5$ (see Table 2) are composed of mainly a mixed phase, a monoclinic phase, and a cubic (or anatase) phase except when $x = 0.3$. When $x = 0.3$, a nearly pure monoclinic phase is formed. When the content of CeO_2 is increased up to $x = 0.6$, the cubic phase is dominant in the $Ce_xTi_{1-x}O_2$ samples.

Figure 2. Rietveld refinement pattern of the Ce$_{0.3}$Ti$_{0.7}$O$_2$ sample. The experimental data are indicated by the dots and the calculated data by the solid line overlaying them. The short vertical lines mark the positions of possible Bragg reflections and the bottom curve shows the difference between the experimental and calculated data.

Table 1. Lattice Parameter and Mean Crystallite Size of Cubic Phase (111) in Ce$_x$Ti$_{1-x}$O$_2$ ($x = 0.4-1.0$)

x	lattice parameter (nm)	mean crystallite size (nm)
0.4	0.535	19.5
0.5	0.534	20.5
0.6	0.538	21.6
0.7	0.537	24.1
0.8	0.539	25.5
0.9	0.539	29.4
1.0	0.543	44.3

Table 2. Phase Composition of Ce$_x$Ti$_{1-x}$O$_2$ Mixed Oxides Based on XRD and Raman Data

x	XRD	Raman
0	rutile, anatase	rutile, anatase
0.1	anatase	anatase
0.2	anatase, monoclinic	anatase, monoclinic
0.3	monoclinic	monoclinic
0.4	cubic, monoclinic	cubic, monoclinic
0.5	cubic, monoclinic	cubic, monoclinic
0.6	cubic	cubic, monoclinic
0.7	cubic	cubic
0.8	cubic	cubic
0.9	cubic	cubic
1.0	cubic	cubic

Table 1 lists the change in the lattice parameter and the mean crystallite size of the cubic phase of Ce$_x$Ti$_{1-x}$O$_2$ in the composition range $0.4 \leq x \leq 1.0$. From Table 1, it can be seen that the lattice parameter of the cubic phase decreases with increasing Ti content. This means that the incorporation of Ti^{4+} ions into the ceria lattice can derive the solid solution of Ce$_x$Ti$_{1-x}$O$_2$ because the radius of Ti^{4+} ions (0.068 nm) is smaller than that of the Ce^{4+} ion (0.094 nm). The mean crystallite size of the cubic phase also decreases with increasing Ti content. This means that the substitution of Ti atoms into the CeO$_2$ lattice inhibits the crystal growth of the cubic phase.

Figure 3 shows the Raman spectra of Ce$_x$Ti$_{1-x}$O$_2$ mixed oxides calcined at 650 °C. There are a number of Raman bands observed at 142, 192, 234, 395, 443, 513, 608, and 634 cm^{-1} for TiO$_2$, which are in good agreement with the Raman spectra of rutile–anatase mixed oxides reported by Busca et al.[23] This result confirms
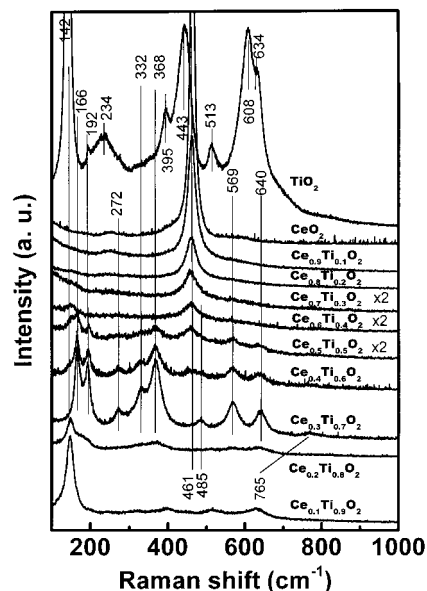

Figure 3. Raman spectra of Ce$_x$Ti$_{1-x}$O$_2$ samples.

that the TiO$_2$ consists of rutile and anatase phases. The spectrum of the Ce$_{0.1}$Ti$_{0.9}$O$_2$ sample resembles the spectral feature of anatase. For the Ce$_{0.3}$Ti$_{0.7}$O$_2$ sample, however, some new Raman bands appear at 166, 192, 272, 332, 368, 485, 596, 640, and 765 cm^{-1}. These Raman bands have never been reported in the literature before. According to the above XRD result, we believe that these new Raman peaks are attributed to the new compound with a monoclinic phase formed by substituting Ce atoms into the TiO$_2$ lattice. However, Ce$_x$Ti$_{1-x}$O$_2$ ($x = 0.7-1.0$) samples give mainly a single sharp band at about 461 cm^{-1}, which is due to the Raman active F_{2g} mode of CeO$_2$, the typical band of a fluorite structural material. The Raman spectra (Figure 3) are consistent with the XRD patterns (Figure 1) of Ce$_x$Ti$_{1-x}$O$_2$ samples.

Table 2 lists the phase composition of Ce$_x$Ti$_{1-x}$O$_2$ mixed oxides on the basis of XPD and Raman results. Compared with the phase composition detected by the two techniques (XRD and Raman), two phases, cubic and monoclinic phase, are detected by Raman spectroscopy for the Ce$_{0.6}$Ti$_{0.4}$O$_2$ sample, and only the cubic phase for the Ce$_{0.6}$Ti$_{0.4}$O$_2$ sample is detected by XRD. This can be attributed to the following two reasons. One is that the X-ray penetrates the bulk of a crystalline particle while the visible laser may not be able to reach the bulk because the Ce$_x$Ti$_{1-x}$O$_2$ absorbs the visible light. So the Raman results may reflect more information from the surface region than XRD. It also indicates that the phase transformation starts at the surface region and then develops toward the bulk for Ce$_x$Ti$_{1-x}$O$_2$ samples. Another reason may be that the relative sensitivities of Raman spectroscopy and XRD are different for some phases.

3.2. Redox Properties. Figure 4 shows the TPR profiles of the Ce$_x$Ti$_{1-x}$O$_2$ mixed oxides. There are two reduction peaks at about 650 and 850 °C in the TPR profiles for Ce$_x$Ti$_{1-x}$O$_2$ ($x = 0.3$), while there is only one peak at 680 °C for the Ce$_{0.2}$Ti$_{0.8}$O$_2$ sample and a weak

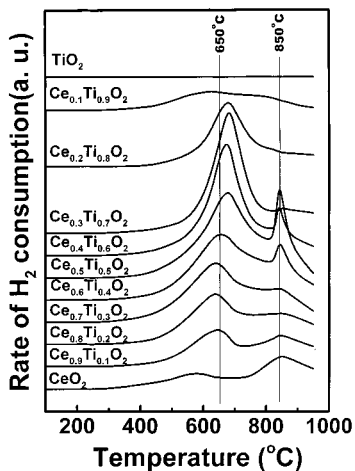(23) Busca, G.; Ramis, G.; Amores, J. M. G.; Escribano, V. S.; Piaggio, P. *J. Chem. Soc., Faraday Trans.* **1994**, *90*, 3181.

Figure 4. TPR profiles of $Ce_xTi_{1-x}O_2$ mixed oxides.

Table 3. Hydrogen Consumption Estimated from Temperature-Programmed Reduction

x	H_2 consumption (mmol/g)^a	composition of reduced sample	
		y in $Ce_xTi_{1-x}O_y{}^b$	y' in $CeO_{y'}-TiO_2{}^c$
0	0	2.00	
0.1	0.356(0.016)	1.97	1.70
0.2	1.072(0.050)	1.90	1.50
0.3	1.250(0.062)	1.86	1.53
0.4	1.920(0.096)	1.79	1.49
0.5	2.144(0.108)	1.73	1.46
0.6	1.964(0.098)	1.73	1.55
0.7	1.830(0.092)	1.73	1.63
0.8	1.428(0.072)	1.78	1.75
0.9	1.384(0.070)	1.78	1.76
1.0	0.580(0.030)	1.90	1.90

^{a} The H_2 consumption was calculated from the integration of TPR area; the numbers in parentheses are error. ^{b} Overall reduction of $Ce_xTi_{1-x}O_2$ mixed oxides. ^{c} Reduction degree of CeO_2 in $Ce_xTi_{1-x}O_2$ mixed oxides.

overlapped peak for $Ce_{0.1}Ti_{0.9}O_2$. TiO_2 does not show an evident reduction peak in the temperature range from 100 to 950 °C. The position of the low-temperature peak, 680 °C, shifts to higher temperatures with increasing TiO_2 content except for the $Ce_{0.1}Ti_{0.9}O_2$ sample, while that of the high-temperature peak remains stable. The intensity of the low-temperature peak increases with increasing TiO_2 content and reaches a maximum at $x = 0.4$. However, the change of the high-temperature peak is very complex. As the x value decreases from 1 to 0.6, the intensity of the high-temperature peak is reduced when $x = 0.4$, 0.5, and 0.6 and this peak grows and becomes very sharp and its intensity reaches a maximum at $x = 0.5$. Two reduction peaks of CeO_2 at about 570 and 850 °C are associated with the stepwise reduction. The peak at 570 °C is generally attributed to reduction in the surface region, and the peak at 860 °C is ascribed to the reduction of bulk. From the relative area of the reduction peak of mixed oxides, the increase in peak area at about 650 °C is attributed to mainly the increase of Ti content in $Ce_xTi_{1-x}O_2$ solid solution. The sharp peak at 850 °C for $Ce_xTi_{1-x}O_2$ samples may be associated with the cubic phase.

Table 3 lists the H_2 consumption of $Ce_xTi_{1-x}O_2$ mixed oxides and the reduction degree of CeO_2 in $Ce_xTi_{1-x}O_2$, supposing that only the CeO_2 component is reduced. The reduction extent of ceria is estimated from the H_2 consumption of the $Ce_xTi_{1-x}O_2$ sample. The H_2 consumption of any $Ce_xTi_{1-x}O_2$ mixed oxide is much higher than
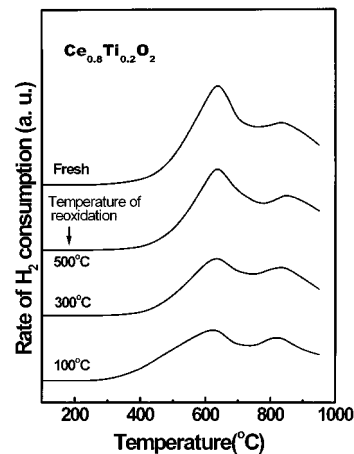

Figure 5. TPR profiles of the $Ce_{0.8}Ti_{0.2}O_2$ sample and the reduced sample reoxidized at different temperatures.
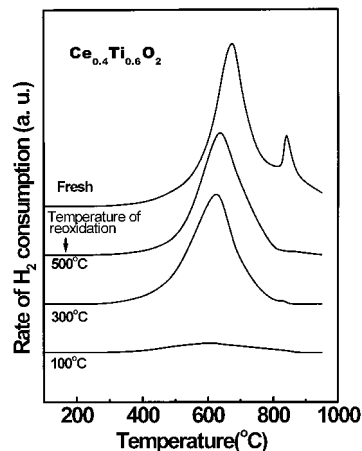

Figure 6. TPR profiles of the $Ce_{0.4}Ti_{0.6}O_2$ sample and reduced sample reoxidized at different temperatures.

that of CeO_2 alone. This means that the presence of TiO_2 promotes the reduction of CeO_2 or the presence of Ti ions weakens the Ce−O bond in the solid solution of $Ce_xTi_{1-x}O_2$ and makes the CeO_2 component more easily reduced. When $x = 0.2-0.6$, the valence value of Ce in the reduced sample of $Ce_xTi_{1-x}O_2$ is estimated to be close to +3, which is much smaller than +3.8 for reduced CeO_2. This indicates that the $Ce_xTi_{1-x}O_2$ solid solution is a potential material with a much higher capability for storage of oxygen.

The redox behavior of CeO_2-TiO_2 mixed oxides is an important feature because most catalysts used for the oxidation reaction are under the redox cycle; for example, a three-way catalyst works under redox conditions. Figures 5 and 6 show the repeated TPR cycles of $Ce_{0.8}Ti_{0.2}O_2$ and $Ce_{0.4}Ti_{0.6}O_2$ samples at different reoxidation temperatures. The TPR peaks become weaker after reoxidation. However, as the temperature of reoxidation treatment decreases, the position of the TPR peak does not change for the $Ce_{0.8}Ti_{0.2}O_2$ sample, whereas it shifts to lower temperatures for the $Ce_{0.4}Ti_{0.6}O_2$ sample. Comparing the peak areas of the fresh and reoxidized samples, we found that H_2 consumption of the reoxidized sample at 500, 300, and 100 °C is about 98, 80, and 80%, respectively, for the first TPR run of the $Ce_{0.8}Ti_{0.2}O_2$ sample and is respectively about 90, 78, and 8% for the $Ce_{0.4}Ti_{0.6}O_2$ sample. This indicates that the reduced $Ce_{0.8}Ti_{0.2}O_2$ sample is easier to be reoxidized
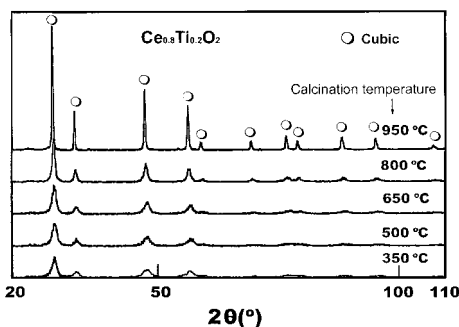
Figure 7. XRD patterns of the Ce$_{0.8}$Ti$_{0.2}$O$_2$ sample calcined at different temperatures.
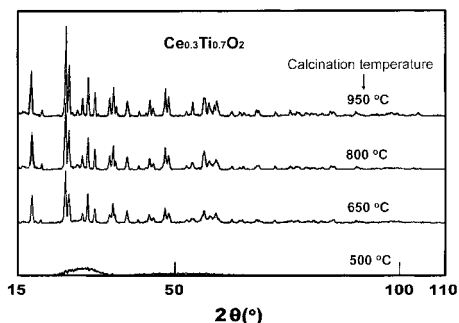

Figure 8. XRD patterns of the Ce$_{0.8}$Ti$_{0.2}$O$_2$ sample calcined at different temperatures.

Figure 9. TPR profiles of the Ce$_{0.8}$Ti$_{0.2}$O$_2$ sample calcined at different temperatures.

Figure 10. TPR profiles of the Ce$_{0.3}$Ti$_{0.7}$O$_2$ sample calcined at different temperatures.

than the reduced Ce$_{0.4}$Ti$_{0.6}$O$_2$ sample. It is worthwhile to notice that the high-temperature peak, 860 °C, is not observed for the reoxidized sample. This indicates that the recovery of the high-temperature peak is difficult with redoxidation.

According to TPR results, we conclude that the introducing of TiO$_2$ into CeO$_2$ leads to the formation of solid solution Ce$_x$Ti$_{1-x}$O$_2$, enhances the reduction of bulk oxygen, and results in high efficiency of the Ce^{4+} $\leftrightarrow$ Ce^{3+} redox cycle, especially, for a CeO$_2$-rich solid solution. In other words, this redox cycle is easier in a cubic-dominant Ce$_{0.8}$Ti$_{0.2}$O$_2$ sample than in the Ce$_{0.6}$Ti$_{0.4}$O$_2$ sample, which is a mixture of cubic and monoclinic phases.

3.3. Phase Stability at Different Calcination Temperatures. Figures 7 and 8 show the XRD patterns of Ce$_{0.8}$Ti$_{0.2}$O$_2$ and Ce$_{0.3}$Ti$_{0.7}$O$_2$ calcined at different temperatures for 4 h. For the Ce$_{0.8}$Ti$_{0.2}$O$_2$ sample (Figure 7), the cubic phase is already formed when the precursor was calcined at 350 °C. However, as the calcination temperature increases, the diffraction peak becomes narrower, which means the crystallite size becomes larger due to the sample sintering. We also found that calcination at higher temperatures does not change the Raman spectra of Ce$_{0.8}$Ti$_{0.2}$O$_2$, as confirmed by the XRD results. For the Ce$_{0.3}$Ti$_{0.7}$O$_2$ sample, the structure of the precursor is still amorphous after calcination at 500 °C (Figure 8). The diffraction peaks of the monoclinic phase are obviously observed after calcination at 650 °C. However, when the calcination temperature is increased from 650 to 950 °C, the position and relative intensity of diffraction peaks no longer change. This means that the monoclinic phase of Ce$_{0.3}$Ti$_{0.7}$O$_2$ mixes oxides has been well derived after calcination at 650 °C. This monoclinic phase is very stable in the temperature range from 650 to 950 °C, and the change of the crystallite size is very small. Figures 9 and 10 show TPR
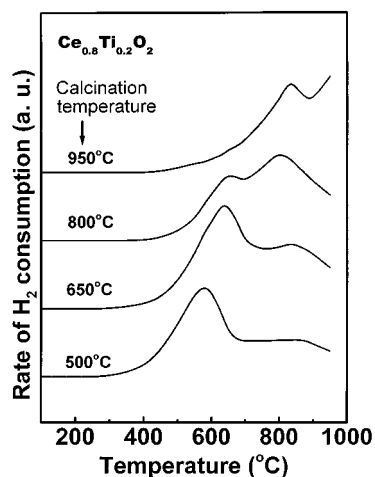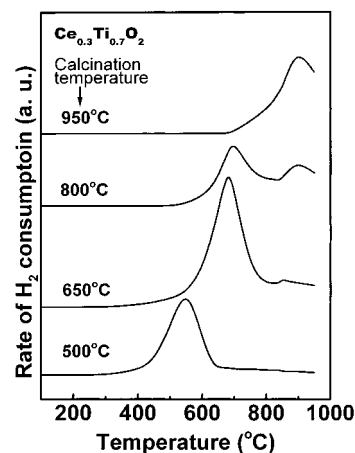
profiles of Ce$_{0.8}$Ti$_{0.2}$O$_2$ and Ce$_{0.3}$Ti$_{0.7}$O$_2$ calcined at different temperatures. As the temperature increases, the peak of TPR shifts to higher temperatures, possibly because of the sintering of the samples.

4. Conclusions

A series of Ce$_x$Ti$_{1-x}$O$_2$ mixed oxides was synthesized by the sol−gel method. XRD and Raman results indicate that the solid solution of Ce$_x$Ti$_{1-x}$O$_2$ is formed via the incorporation of TiO$_2$ into a CeO$_2$ lattice. A solid solution of Ce$_x$Ti$_{1-x}$O$_2$ with a cubic phase is detected when $x \geq$ 0.6 and a mixture phase for $x \leq 0.5$ samples. When $x =$ 0.3, a monoclinic phase is observed with the space group $C2/m$ and $a = 0.9811(8)$ nm, $b = 0.3726(3)$ nm, $c = 0.6831(6)$ nm, and $\beta = 118.84°$. The lattice parameter and the mean crystallite size of the cubic phase decreases with increasing Ti content. This means that the incorporation of the Ti ion into a CeO$_2$ lattice inhibits the crystal growth of the cubic phase. The crystallite phases of Ce$_x$Ti$_{1-x}$O$_2$ are shown to be stable at calcination temperatures from 500 to 950 °C.

The reduction degree of Ce$_x$Ti$_{1-x}$O$_2$ is greatly enhanced, owing to the introduction of Ti into a CeO$_2$ lattice. For Ce$_x$Ti$_{1-x}$O$_2$ ($x = 0.2−0.6$) samples, the Ce^{4+} ions reduced at 950 °C are estimated to be about Ce^{3+}, while the reduction of CeO$_2$ alone at 950 °C can reach only Ce$^{3.8+}$. The reduced Ce$_x$Ti$_{1-x}$O$_2$ mixed oxides can

be easily oxidized, indicating that the new material possesses excellent redox properties. The CeO_2-rich solid solution shows better oxygen storage than the CeO_2-lean solid solution.

CM000470S